Solar Energy 174 (2018) 549–555

Contents lists available at ScienceDirect

Solar Energy

journal homepage: www.elsevier.com/locate/solener

14.1% efficiency hybrid planar-Si/organic heterojunction solar cells with SnO_2 insertion layer

Lei Chen[a], Zhongliang Gao[a], Yupeng Zheng[b], Mengqi Cui[b], Hejin Yan[b], Dong Wei[b], Shangyi Dou[b], Jun Ji[b], Endong Jia[c], Na Sang[a], Kunhao Liu[b], Xunlei Ding[a], Yingfeng Li[b], Meicheng Li[b,*]

[a] School of Mathematics and Physics, North China Electric Power University, Beijing 102206, China
[b] State Key Laboratory of Alternate Electrical Power System with Renewable Energy Sources, School of Renewable Energy, North China Electric Power University, Beijing 102206, China
[c] Key Laboratory of Solar Thermal Energy and Photovoltaic System, Institute of Electrical Engineering, Chinese Academy of Sciences, Beijing 100190, China

ARTICLE INFO

Keywords:
Si/organic heterojunction solar cells
Stannic oxide
Insertion layer
Density functional theory

ABSTRACT

Hybrid planar-Si/organic heterojunction solar cells have gained considerable interest in the fabrication of cost-effective and high-efficiency devices. However, most of high power conversion efficiency (PCE) performances have been obtained with particular structures, front surface texture or rear surface field layer. In this paper, we provide a simple method without complex structures, and demonstrate the superiority and the mechanism of using stannic oxide (SnO_2) as an insertion layer. The SnO_2 insertion layer takes the place of the Schottky barrier, which reduces barrier height of rear Si to enhance charge transfer. And the effect of the insertion layer reduces contact resistance and enhances contact quality of rear Si side. Meanwhile, it has been indicated that the Si-O-Sn bonds were formed by SnO_2 and Si dangling bond (Si-), which have a passivation effect on the Si surface to effectively suppress the recombination losses. Furthermore, simulations using density functional theory (DFT) confirm that the electrostatic potential can improve electronic transmission from Si to Sn between Si-O-Sn bonds. Finally, for the hybrid planar-Si/PEDOT:PSS heterojunction solar cells without any special structures, the highest PCE of 14.1% was achieved, up 10.8% compared with that without SnO_2 insertion layer. These findings provide an effective way of improving Si/metal contact via a simple, room temperature process for other photovoltaic devices.

1. Introduction

Silicon (Si)/organic heterojunction solar cells made of a poly (3,4-ethylenedioxythiophene); poly(-styrenesulfonate) (PEDOT:PSS), on Si have gained considerable interest in the fabrication of cost-effective and high-efficiency devices (He et al., 2012; Thomas and Leung, 2014). The heterojunction between Si surface and PEDOT:PSS film separates and extracts photogenerated electrons-holes, which were formed by a simple spin-coating method in room temperature. In order to improve the performance of Si/PEDOT:PSS heterojunction solar cells, light-harvest texture, surface passivation, modification of PEDOT:PSS solution and ultrathin Si substrate were studied (Bai et al., 2012a, 2013, 2012b; Ding et al., 2014; Duan et al., 2014; Geng et al., 2012; Li et al., 2016; Tecedor et al., 2018). At present, the power conversion efficiency (PCE) of Si/PEDOT:PSS heterojunction solar cells is up to ~16%, which has not surpassed that of the traditional homojunction Si solar cells (He et al., 2017a, 2018). However, the traditional homojunction Si solar cells have the inborn disadvantages of pollution and energy consumption. The advantages of Si/PEDOT:PSS heterojunction solar cells can compensate for the shortage of its PCE, and it has significance to be researched in the future.

Although PCE of Si/PEDOT:PSS heterojunction solar cells has been greatly improved, there are many problems between rear Si and electrode still to be solved (Han et al., 2017). The Schottky barrier reduces the collection of electrons and increases the surface carrier recombination in rear Si to jeopardize the performance of the solar cell (Huang et al., 2007). This matter draws many research groups' attention who have achieved fruitful results (Devkota et al., 2016; Han et al., 2017; He et al., 2017b; J. Liu et al., 2017; Y. Liu et al., 2017; Liu et al., 2016; Tong et al., 2018; Xia et al., 2017). A traditional method of Ohmic contact between Al and Si via high doping in Si side is generally used to improve the electrical contact properties. However, this process requires high temperature (~800 °C) as well as toxic gases, such as diborane or phosphine, which are similar to the disadvantages in

* Corresponding author.
E-mail address: mcli@ncepu.edu.cn (M. Li).

https://doi.org/10.1016/j.solener.2018.09.035
Received 20 July 2018; Received in revised form 19 August 2018; Accepted 13 September 2018

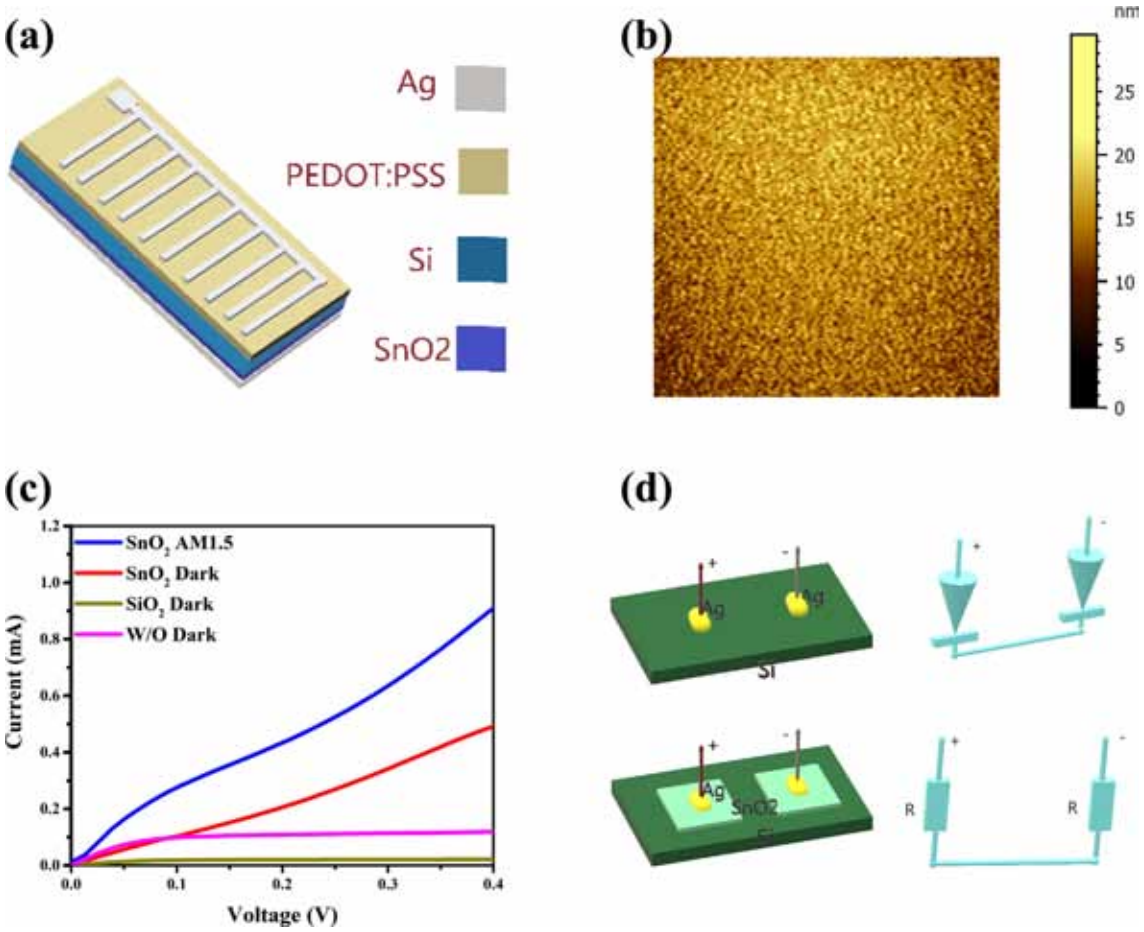

Fig. 1. (a) scheme of Hybrid planar-Si/PEDOT:PSS heterojunction solar cell with SnO_2 layer. (b) AFM of SnO_2 film under the Si substrate with scan size of 6 × 6 μm. (c) I-V curves of photodetector devices based on SnO_2, SiO_2 and without both in the dark and under AM 1.5G illumination. (d) The device structure diagram and equivalent circuit diagram of current-voltage (I-V) testing.

traditional homojunction Si solar cell (He et al., 2017a). As an alternative, n-type polymers (PCBM, N2200 and F-N2200) and alkali metal salts (LiF, Cs_2CO_3) have been used to improve contact quality between rear Si and electrode (Devkota et al., 2016; Han et al., 2017; Lee et al., 1998; J. Liu et al., 2017; Zhang et al., 2015). These materials can be deposited between rear Si and electrode by solution method that has a simple process with low temperature (< 120 °C). Solution method is better than that with toxic gases. Although the problem of rear Si has been solved through these materials as insertion layer, these materials are not perfect due to a matter of band structure or stability. Metal oxide materials with wide band gaps are suitable insertion layer materials to transmit of electrons and block holes. Stannic oxide (SnO_2) is a typical metal oxide with wide band gap as an intercalation layer, which has suitable energy levels with the conduction band (Ec) of 4.30 eV and valence band (Ev) of 8.09 eV. And the chemical bonds are produced between this material and Si surface to reduce the dangling bonds and surface recombination.

In this paper, we deposited SnO_2 insertion layer between rear Si and electrode by a solution method which takes the place of the Schottky barrier to reduce contact resistance. The band structure of SnO_2 is measured by ultraviolet photoelectron spectroscopy (UPS) and suitable for selective transmission of electrons and holes. The simulations using density functional theory (DFT) confirm that the electrostatic potential can improve electronic transmission by Si-O-Sn bonds. It has been found that, those bonds enhance Si surface passivation and suppress the recombination losses to improve short-circuit current (I_{sc}). The open-circuit voltage (V_{oc}) of 593 mV with a highest PCE of 14.1% was achieved from planar-Si/PEDOT:PSS heterojunction solar cells just by adding SnO_2 insertion layer.

2. Experimental section

2.1. Materials and devices fabrication

The planar-Si/PEDOT:PSS heterojunction solar cells were fabricated on one side polishing n-type Si (1 0 0) substrates (Phosphorus doped), with resistivity of 2–4 Ω·cm and thickness of 500 μm (Tianjin Upward Technology Development Co., Ltd). The substrates were cut into 1.5 × 1.5 cm^2 and ultrasonically cleaned for 10 min successively in acetone, ethanol and deionized (DI) water. After cleaning, the substrates were immersed in 5% hydrofluoric acid (HF) for 3 min to remove the native oxide and then thoroughly cleaned in DI water. We diluted raw SnO_2 solution (alfa) with DI water which was mixed with 0.1 wt% Triton (Alfa, TX-100). The diluted SnO_2 solution was spin-coated onto rear silicon surface at 3000 rpm and then annealed at 120 °C for 8 min, and 100 nm thick Ag film was deposited onto the rear silicon by magnetron sputtering. PEDOT:PSS (Heraeus, PH1000) solution was mixed with 5 wt% dimethyl sulfoxide (innochem, DMSO) and 0.25 wt% TX-100, and then stirred for several hours with magnetic force. The processed PEDOT:PSS solution was spin-coated onto front silicon surface at 5000 rpm and then annealed at 120 °C for 15 min, and 200 nm thick Ag grid electrode was deposited onto the PEDOT:PSS layer through a shadow mask by magnetron sputtering. Finally, the cell was cut into 0.7 × 0.4 cm^2 for testing, whose active area was about 0.20 cm^2 after subtracting Ag grid electrode from it.

Table 1
Electrical output characteristics of devices with different device structures, data based on five cells of each type.

Device structure	V_{oc} (mV)	J_{sc} (mA·cm^{-2})	FF	PCE (%)
SnO_2	593 (592 ± 3)	33.16 (33.41 ± 0.92)	0.72 (0.70 ± 0.01)	14.16 (13.95 ± 0.55)
W/O SnO_2	582 (576 ± 5)	31.85 (30.80 ± 1.18)	0.68 (0.69 ± 0.01)	12.77 (12.35 ± 0.51)

2.2. Device characterization

J-V characteristics were tested by a solar simulator (Keithley 2400, AM 1.5G, 100 mW/cm^2). EQE spectra and reflectivity were measured by Zolix SCS100 full function solar cell quantum efficiency test system. I-V curves of Ag-SnO_2 layer-Si or Ag-Si were measured by Keithley 2400 system. The minority carrier lifetimes were measured by microwave-detected photoconductivity Semilab WT-2000 system. The AFM map of SnO_2 film was measured by Aglient Keysight AFM-5500. The SEM map of PEDOT:PSS film was measured by HITACHI SU8010. UPS and XPS were measured by ESCALAB 250Xi, Thermofisher Scientific.

3. Results and discussion

We assembled the structure of planar-Si/PEDOT:PSS heterojunction solar cells as shown in Fig. 1(a). Although the PCE of 12.7% was achieved in the structure without SnO_2 insertion layer as shown in Table, there is a disadvantage between rear Si and electrode. The existence of Si and metal contacts on the rear Si produces a Schottky barrier that can spoil the performance. When metal and Si form a junction, the surface state on Si surface should be considered and we can illustrate the process of forming a junction by Fig. 2(a)–(c). First, the three systems are electrically neutral before contact, and the surface state is in the band gap of Si in Fig. 2(a). Then, the metal and the surface state are the first to be bonded, and the electrons in the metal flow to the surface state, reducing the Fermi Energy (E_F) of the metal and raising the E_F of the surface state, and Fig. 2(b) illustrates the situation. Finally, the system composed of metal and surface state is bonded with Si, and the electrons in the Si flow to the system, reducing the E_F of Si and raising the E_F of the system, as shown in Fig. 2(c). The equivalent energy band diagram of forming Schottky barrier is shown in Fig. 2(d). The electrons in Si flows to the metal only through the way of thermionic emission, which is difficult to transmit electrons. A traditional approach to Ohmic contact via high doping Si side is used to improve the electron transmission, and the equivalent energy band diagram is shown in Fig. 2(e). The electrons can easily flow to the metal through tunneling, because the space-charge region becomes thinner in Ohmic contact, and the energy band bending is advantageous to holes to flow to metal. However, electrons should have flowed to metal electrodes, and holes should have flowed to the PEDOT:PSS layer in Si/PEDOT:PSS heterojunction. We need an energy band structure to transmit electron barrier holes in rear Si, rather than simply enable current transfer, such as Ohmic contact. We studied the SnO_2 insertion layer between rear Si and electrode and proved the perfect energy band structure of transmitting electron blocking holes as shown in Fig. 2(f).

We can see the structure of planar-Si/PEDOT:PSS heterojunction solar cell in Fig. 1(a). The electron-hole separation area is between front Si surface and the PEDOT:PSS layers. Contact quality of Si and PEDOT:PSS layer is very important for the solar cells. Fig. S1 is the SEM image of the contact between the silicon and the PEDOT:PSS layer by spin-coating, whose thickness is about 74 nm. Fig. 1(b) shows AFM of SnO_2 layer which is deposited by spin coating on the silicon surface. Fig. S2 shows high resolution AFM three-dimensional image of SnO_2 layer on the silicon surface. We can get the mean square value of the surface roughness (RMS = 2.47 nm) of SnO_2 layer, which proves that the surface quality of SnO_2 layer is improved.

We demonstrate that the effect of SnO_2 insertion layer between rear Si and electrode substitutes the Schottky barrier. In order to explore the mechanism of the SnO_2 insertion layer in the planar-Si/PEDOT:PSS heterojunction solar cells, we designed three kinds of structural device for current-voltage (I-V) testing, as shown in Fig. S3, which are Ag-Si, Ag-SiO_2-Si and Ag-SnO_2-Si devices. Fig. 1(d) shows the equivalent circuit diagrams of two devices that are two reverse diodes and resistances in series. I-V curves in different devices are shown in Fig. 1(c). The I-V curve of Ag-Si device indicates the existence of the Schottky barrier whose height is about 0.56–0.76 eV, which blocks electron transmission between rear Si and electrode in solar cells (Huang and Hai, 1979). The SiO_2 layer about 2 nm was added between Si and Ag in a natural oxidation method, which can reduce the Schottky barrier and promote electron transmission (He et al., 2012). However, SiO_2 layer is an insulator and increases the contact resistance to reduce the current in Fig. 1(c). The SnO_2 is a semiconductor which has better conductivity than that of SiO_2. The I-V curve of the Ag-SnO_2-Si device does not have the characteristics of the Schottky barrier, which can prove that there is no Schottky barrier. At the same time, we have proved that the electronic conductivity of the Ag-SnO_2-Si device not only reduce the barrier height or shorten the space-charge region to realize the electron tunneling simply, but also there is selective transmission which can transmit electrons and block holes.

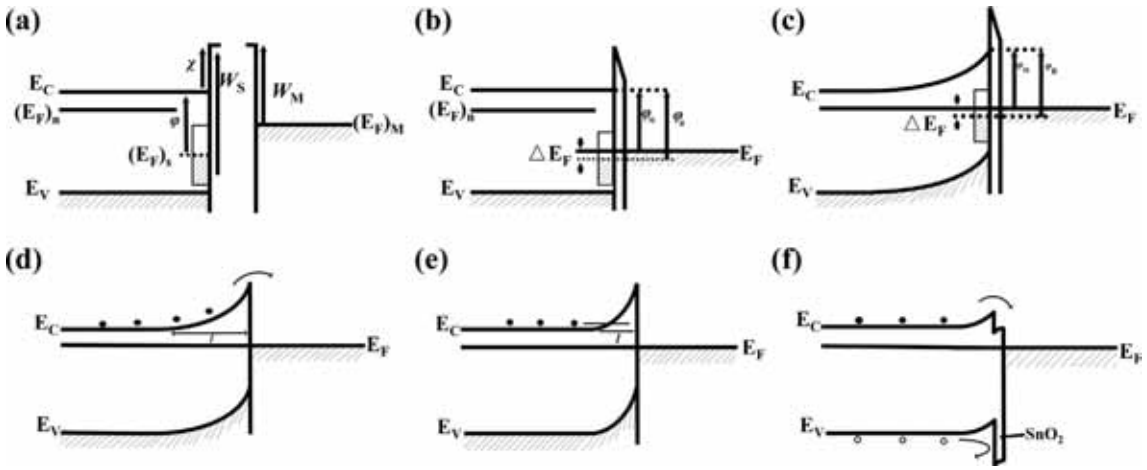

Fig. 2. (a)–(c) the energy band structure diagram of the Schottky barrier formation process. (d) the energy band structure diagram of the Schottky contact. (e) the energy band structure diagram of Ohmic contact. (f) the energy band structure diagram of metal and Si contact with SnO_2 insertion layer.

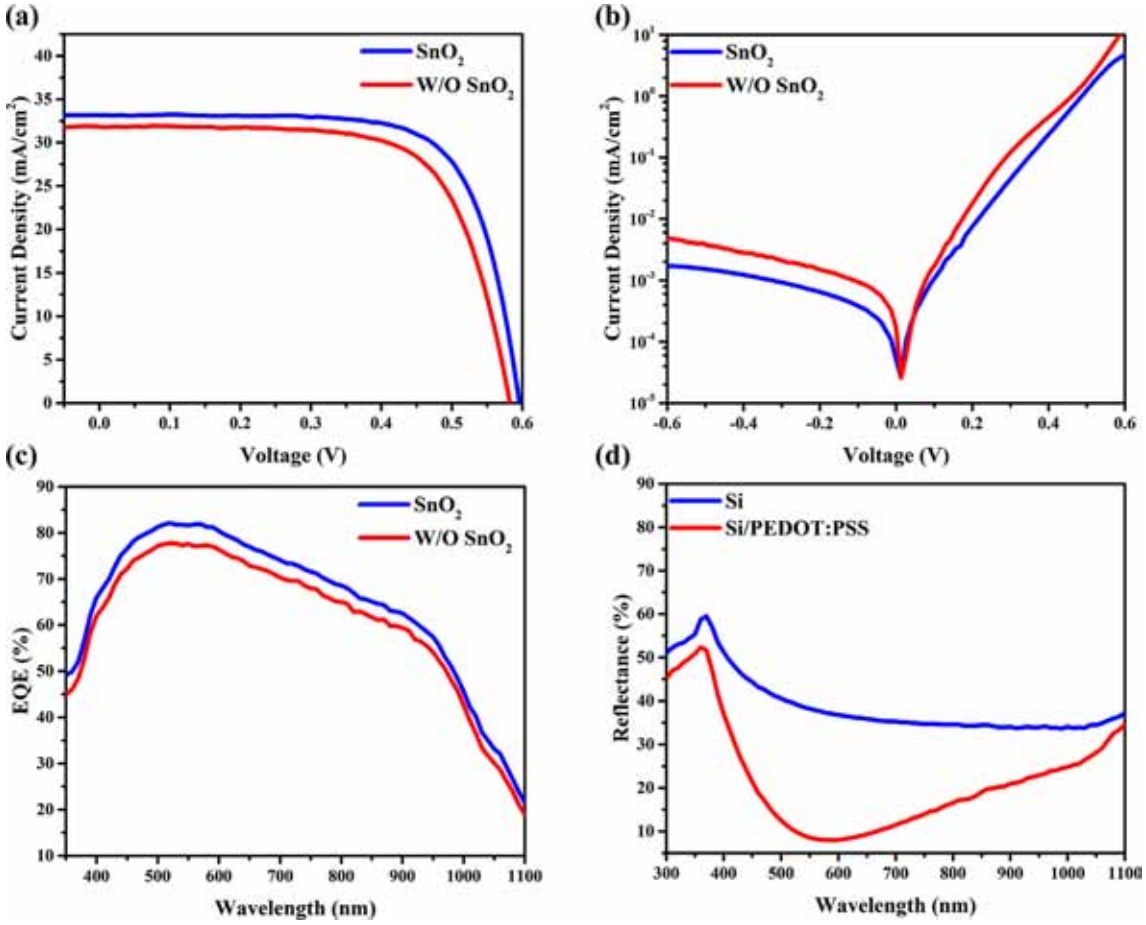

Fig. 3. (a) J_{sc}-V curves under solar-simulated AM1.5G light illumination at 100 mW·cm^{-2}. (b) J_0-V curves in the dark. (c) EQE spectra of the device of with and without SnO_2 layer. (d) The relationship between reflectivity and wavelength of device with PEDOT:PSS and without PEDOT:PSS.

According to the assembly diagram shown in Fig. 1(a), the PCE of the device with SnO_2 layer is superior to that of device without SnO_2 layer. Under AM 1.5G illumination, current density versus voltage (J-V) curves of devices made with and without SnO_2 layer were plotted in Fig. 3(a). The device structure with SnO_2 layer yielded an eximious PCE of 14.16% which has been increased by 10.8% with a high V_{oc} of 593 mV, a short-circuit current density (J_{sc}) of 33.16 mA·cm^{-2} and a fill factor (FF) of 0.72. Electrical output characteristics of devices with different device structure were summarized in Table 1. The V_{oc}, J_{sc} and FF are increased in the comparison of two groups of data.

The SnO_2 insertion layer can reduce the barrier height in rear Si to raise V_{oc} of Si/PEDOT:PSS heterojunction solar cell. We applied UPS testing methods to get energy band information, which can prove that the voltage is raised by a quantitative method. UPS information of cutoff edge and Ev spectra of SnO_2 and SiO_2 were shown in Fig. 4(a) and (b), respectively. These Figs illustrate that the work function (W_s), and valance band maximum (VBM) of the SnO_2 are 4.39 eV and 3.7 eV. The bandgap (E_g) is 3.79 eV from other groups work (Jiang et al., 2016). It can be calculated that the E_C of the SnO_2 is 4.30 eV, as obtained from $E_C = W_s + VBM - E_g$ based on the semiconductor band structure in Fig. S6. The band energy diagram can be drawn according to these parameters in Fig. 2(d) and (f). The Ag-Si device has a Schottky barrier (V_s), with a barrier height of about 0.6 eV (Huang and Hai, 1979). And the Ag-SnO_2-Si device has a barrier (V_b), with a barrier height of about 0.1 eV. The V_{oc} can be proved to be improved by comparing V_s and V_b.

There is a correlation between voltage and current. Higher V_{oc} can be obtained by higher photocurrent and dark current density ratio (J_{sc}/J_0). The equation of V_{oc} is as follows:

$$V_{oc} = \frac{KT}{q}\ln\left(\frac{J_{sc}}{J_0} + 1\right) \quad (1)$$

where K is Boltzmann's constant, q is electron charge, and T is temperature. The transmission of electrons to the Ag electrode needs to overcome V_s without SnO_2 insertion layer, and the hole transmission is very easy, as shown in Fig. 2(d). The transmission of electrons to the Ag electrode is easy to overcome V_b with SnO_2 insertion layer, and the hole transmission needs to overcome the barrier of about 3 eV, which is very difficult, as shown in Fig. 2(f). From the view of transmission electron hole, the Ag-SnO_2-Si device structure achieves the function of transmitting electron and blocking holes, which can prove that J_{sc} is improved. The J_{sc}-V and J_0-V curves of devices made with and without SnO_2 layer in the dark are plotted in Fig. 3(a) and (b), respectively. The J_0 of device with SnO_2 layer is lower than that of device without SnO_2 layer. A higher V_{oc} can be proved according to the Eq. (1) with J_{sc} and J_0 when SnO_2 insertion layer is added.

During the assembly process, chemical bonds between Si and SnO_2 were broken and recombined to form Si-O-Sn bonds. We deposited the SnO_2 film by the spin-coating method and heated it, which may cause break and recombination of chemical bonds. To explore whether SnO_2 and Si are bonded in the form of chemical bonds, an X-ray photoelectron spectroscopy (XPS) method was used. The XPS measurements of Si (2P) peaks for bare Si without SiO_2 and with SnO_2 are shown in Fig. 4(c) and (d). In the Fig. 4(c), the peak of 102.7 eV is Si-O-Si bond when the bare Si is oxidized (Sahasrabudhe et al., 2015). In the Fig. 4(d), when a SnO_2 layer is deposited on the bare Si substrate, it also has a peak of 102.7 eV, and there are two peaks of 102.09 eV and 101.37 eV, respectively. In the Fig. 4(c) and (d), Si substrate and

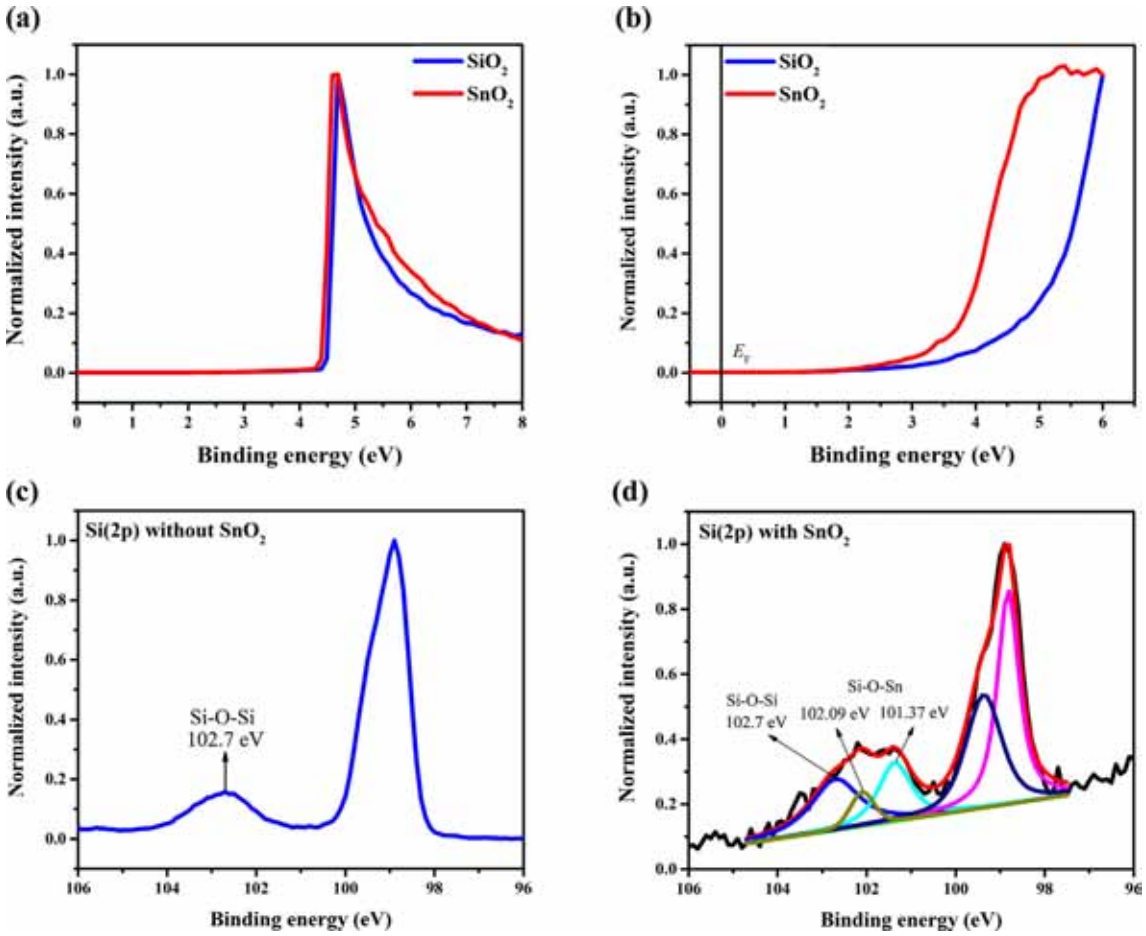

Fig. 4. (a) ultraviolet photoelectron spectroscopy (UPS) cutoff edge of SnO_2 (red), SiO_2 (black). (b) valence band spectra of SnO_2 (red), SiO_2 (black) from UPS measurements. (c)X-ray photoelectron spectroscopy (XPS) measurements of Si(2P) peaks for bare Si substrate with SiO_2. (d) XPS measurements of Si(2P) peaks for bare Si substrate with SnO_2 layer. (For interpretation of the references to color in this figure legend, the reader is referred to the web version of this article.)

processing technology are same, and only SnO_2 is different. So, in Fig. 4(d), the peak of 102.7 eV is Si-O-Si band, the peaks of 102.09 eV and 101.37 eV are two forms of Si-O-Sn band. DFT simulations show that Si, O and Sn interact with each other, proving the possibility of chemical bonds. Fig. 5(a) is a model of Si and SnO_2 structures which are obtained from the bulk material. Their structural optimization, charge distribution and electrostatic potential distribution are calculated, as shown in Fig. 5(b)–(e) and (g).

Si-O-Sn bonds are beneficial to the transmission of electrons from Si to Sn. Fig. 5(g) shows that the charge distribution and electrostatic potential distribution of a cross section is from Fig. 5(e). Si and Sn are linked with O, whose charge are 0.342 e and 1.658 e, respectively. Fig. 5(f) is drawn according to the charge distribution between Si and SnO_2, which proves the transmission of electrons from Si to Sn. In the light of the solar cell, the electrons in the rear Si surface must be transferred to SnO_2 to produce current. The quantum efficiency (QE) is used to explain the relationship between the photocurrent and the incident light. External quantum efficiency (EQE) spectra of the device with and without SnO_2 layer is shown in Fig. 3(c). The relationship between the J_{sc} and EQE follows the equation:

$$\mathrm{EQE} = \frac{J_{sc}}{qQ} \tag{2}$$

where Q is spectral density of incident photon. It can be seen from Fig. 3(c) that the EQE of devices with SnO_2 layer is higher than that of device without SnO_2 layer, which can also prove that the J_{sc} is improved by Si-O-Sn bonds. The other one, internal quantum efficiency (IQE) is plotted in absorption lengths of device with and without SnO_2 layer. The relationship between IQE and EQE follows the equation:

$$\mathrm{IQE} = \frac{EQE}{1-R} \tag{3}$$

where R is reflectivity. Reflectivity versus wavelength curve of device with PEDOT:PSS and without PEDOT:PSS are plotted in Fig. 3(d). The PEDOT:PSS layer has antireflective effects, especially in the range of 450–800 nm. The IQE is obtained by R and EQE as shown in Fig. S5. IQE of device with SnO_2 layer is better than that of device without SnO_2 layer. The J_{sc} of device with SnO_2 layer can be higher, which is consistent with the conclusion of EQE.

Si-O-Sn bonds affect the surface passivation by reducing surface state density, reduce recombination rate and enhance the Minority carrier lifetime (τ_{eff}). The recombination rate of non-equilibrium carriers determines the output current and PCE. In order to get more current, we attempt to reduce the recombination rate, and the τ_{eff} is defined as follows:

$$\tau = \frac{1}{N_t r_+} \tag{4}$$

where N_t and r_+ are the number and coefficient of capturing holes in recombination center, respectively. The surface state is deep in the band gap, which is an efficient recombination center (Huang and Hai, 1979). DFT simulations show that Si-O-Sn bonds lead into a series of gap states in the band gap and form a continuous energy band to reduce the position Ec (Wan et al., 2017). Some surface states are changed by Si-O-Sn bonds, which reduces surface state density to enhance the τ_{eff}. And τ_{eff} was measured by microwave photo conductivity decay (μ-

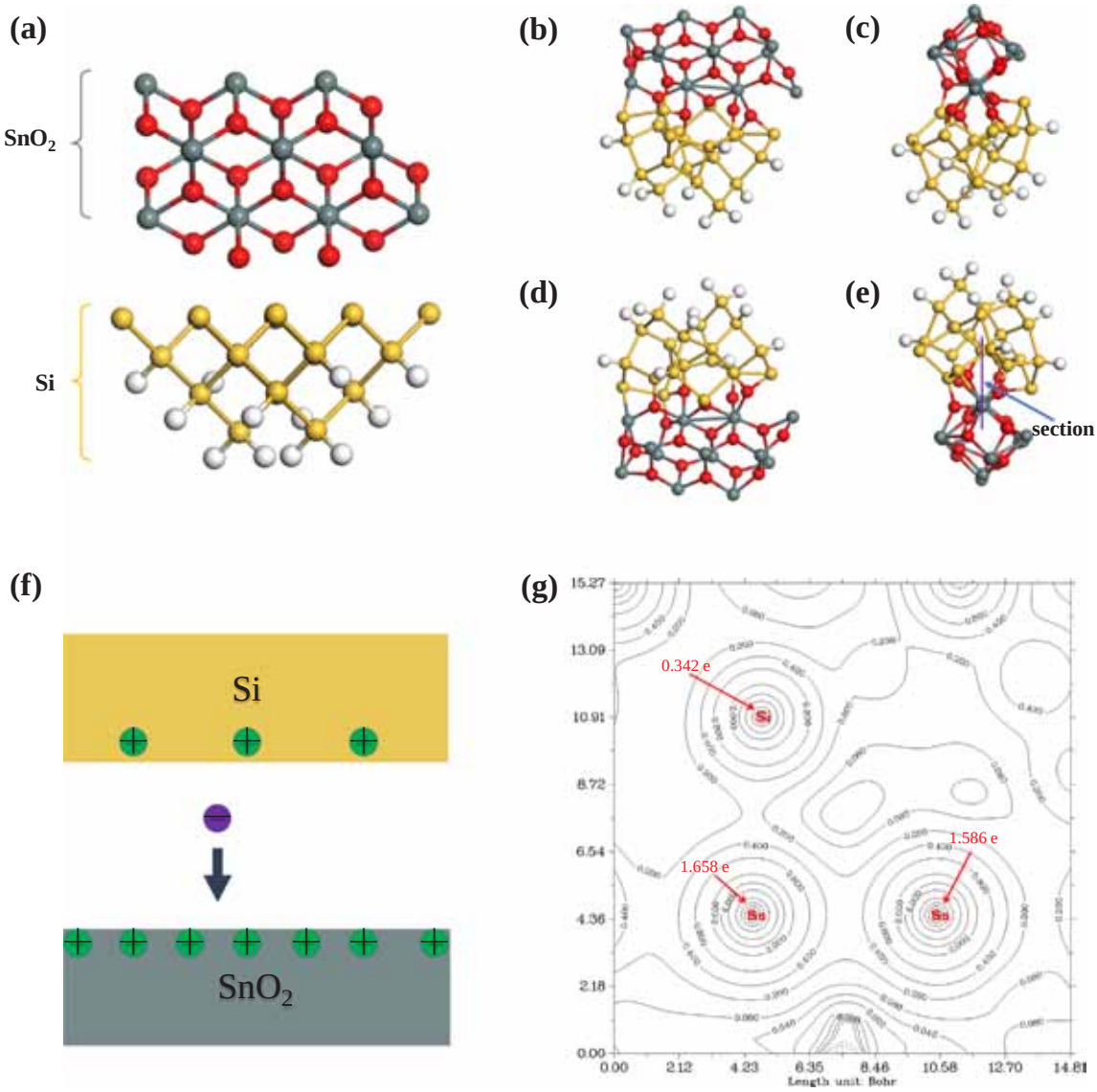

Fig. 5. (a) the model of SnO_2 and Si in DFT simulation. (b), (c), (d) and (e) the result of optimized geometries. (f) schematic diagram of charge distribution between Si and SnO_2. (g) electrostatic potential distribution of cross section represented by purple line in (e), red numbers represent atomic electricity. (For interpretation of the references to color in this figure legend, the reader is referred to the web version of this article.)

PCD). The τ_{eff} follows an equation:

$$\frac{1}{\tau_{eff}} = \frac{1}{\tau_{bulk}} + \frac{S_{eff1} + S_{eff2}}{d} \quad (5)$$

where τ_{bulk} is bulk Si lifetime, d is Si substrate thickness, and S_{eff1} and S_{eff2} are the Si front and rear surface recombination velocity respectively. In Eq. (5), the τ_{bulk}, d and S_{eff1} are constant with the same Si substrate. The S_{eff2} represents rear Si surface quality, which is related to τ_{eff}. The τ_{eff} histograms of Si with SiO_2 and SnO_2 were shown in Figs. S7 and S8, respectively. From the histogram, the mean value of τ_{eff} of Si with SiO_2 is below 21 μs, and the mean value of τ_{eff} of Si with SnO_2 is over 21 μs. Compared with Fig. S7 and Fig. S8, the τ_{eff} of Si with SnO_2 is higher than that of Si with SiO_2, and the Si of SnO_2 surface quality is improved.

We can also obtain that the W_s and VBM of SiO_2 are 4.49 eV and 5.13 eV, respectively. The insertion of the SiO_2 layer between the rear Si and the Ag electrodes can reduce the Schottky barrier, which can improve the performance of the solar cell. However, the SiO_2 is an insulator with a large resistance in solar cell. When the SiO_2 insertion layer reaches a certain thickness, adding it is equal to the introduction of a larger resistance which reduce the performance of solar cell. Therefore, the Ag-SiO_2-Si device structure is not the best choice.

4. Conclusion

We first introduce the SnO_2 insertion layer into these solar cells with a simple method to avoid the particular structures. The mechanism of contact between this layer and rear Si surface was studied, which includes the change of band structure and the formation of Si-O-Sn bonds to enhance the performance of solar cells. The band structure was changed, including the replacement of the Schottky barrier and the reduction of the barrier height, to achieve the effect of transmitting electrons and blocking holes. DFT simulations show the Si-O-Sn bonds electrostatic potential distribution to prove that electrons are easily transmitted from Si to Sn. Meanwhile, the hybrid plana-Si/PEDOT:PSS heterojunction solar cells with SnO_2 insertion layer was fabricated by a simple and room temperature method and has advantages over specific structures. Finally, a PCE of 14.1% with SnO_2 insertion layer was achieved, which is an excellent choice for improving the performance of the Si substrate solar cells.

Acknowledgments

This work is supported partially by National Natural Science Foundation of China (Grant nos. 51772096), Beijing Natural Science Foundation (L172036), Joint Funds of the Equipment Pre-Research and Ministry of Education (6141A020225), Par-Eu Scholars Program, Science and Technology Beijing 100 Leading Talent Training Project, Beijing Municipal Science and Technology Project (Z161100002616039), the Fundamental Research Funds for the Central Universities (2016JQ01, 2017ZZD02) and the NCEPU "Double First-Class" Graduate Talent Cultivation Program.

Appendix A. Supplementary material

Supplementary data to this article can be found online at https://doi.org/10.1016/j.solener.2018.09.035.

References

Bai, F., Li, M., Huang, R., Song, D., Jiang, B., Li, Y., 2012a. Template-free fabrication of silicon micropillar/nanowire composite structure by one-step etching. Nanoscale Res. Lett. 7 (1), 557.

Bai, F., Li, M., Huang, R., Yu, Y., Gu, T., Chen, Z., Fan, H., Jiang, B., 2013. Wafer-scale fabrication of uniform Si nanowire arrays using the Si wafer with UV/Ozone pre-treatment. J. Nanopart. Res. 15 (9).

Bai, F., Li, M., Song, D., Yu, H., Jiang, B., Li, Y., 2012b. One-step synthesis of lightly doped porous silicon nanowires in $HF/AgNO_3/H_2O_2$ solution at room temperature. J. Solid State Chem. 196, 596–600.

Devkota, R., Liu, Q., Ohki, T., Hossain, J., Ueno, K., Shirai, H., 2016. Solution-processed crystalline silicon double-heterojunction solar cells. Appl. Phys. Express 9 (2), 022301.

Ding, R., Dai, H., Li, M., Huang, J., Li, Y., Trevor, M., Musselman, K.P., 2014. The application of localized surface plasmons resonance in Ag nanoparticles assisted Si chemical etching. Appl. Phys. Lett. 104 (1).

Duan, Z., Li, M., Mwenya, T., Bai, F., Li, Y., Song, D., 2014. Geometric parameter optimization to minimize the light-reflection losses of regular vertical silicon nanorod arrays used for solar cells. Phys. Stat. Solidi A 211 (11), 2527–2531.

Geng, X., Qi, Z., Li, M., Duan, B.K., Zhao, L., Bohn, P.W., 2012. Fabrication of antireflective layers on silicon using metal-assisted chemical etching with in situ deposition of silver nanoparticle catalysts. Sol. Energy Mater. Sol. Cells 103, 98–107.

Han, Y., Liu, Y., Yuan, J., Dong, H., Li, Y., Ma, W., Lee, S.-T., Sun, B., 2017. Naphthalene diimide-based n-type polymers: efficient rear interlayers for high-performance silicon-organic heterojunction solar cells. ACS Nano 11 (7), 7215–7222.

He, J., Gao, P., Yang, Z., Yu, J., Yu, W., Zhang, Y., Sheng, J., Ye, J., Amine, J.C., Cui, Y., 2017a. Silicon/organic hybrid solar cells with 16.2% efficiency and improved stability by formation of conformal heterojunction coating and moisture-resistant capping layer. Adv. Mater. 29 (15).

He, J., Ling, Z., Gao, P., Ye, J., 2017b. TiO_2 films from the low-temperature oxidation of Ti as passivating-contact layers for Si heterojunction solar cells. Sol. RRL 1 (12).

He, J., Wan, Y., Gao, P., Tang, J., Ye, J., 2018. Over 16.7% efficiency organic-silicon heterojunction solar cells with solution-processed dopant-free contacts for both polarities. Adv. Funct. Mater.

He, L., Jiang, C., Wang, H., Lai, D., Rusli, 2012. High efficiency planar Si/organic heterojunction hybrid solar cells. Appl. Phys. Lett. 100 (7).

Huang, J., Xu, Z., Yang, Y., 2007. Low-work-function surface formed by solution-processed and thermally deposited nanoscale layers of cesium carbonate. Adv. Funct. Mater. 17 (12), 1966–1973.

Huang, K., Hai, R., 1979. Elementary Semiconductor Physics. Science Press, China.

Jiang, Q., Zhang, L., Wang, H., Yang, X., Meng, J., Liu, H., Yin, Z., Wu, J., Zhang, X., You, J., 2016. Enhanced electron extraction using SnO_2 for high-efficiency planar-structure $HC(NH_2)_2PbI_3$-based perovskite solar cells. Nat. Energy 2 (1).

Lee, S.T., Hou, X.Y., Mason, M.G., Tang, C.W., 1998. Energy level alignment at Alq/metal interfaces. Appl. Phys. Lett. 72 (13), 1593–1595.

Li, Y., Fu, P., Li, R., Li, M., Luo, Y., Song, D., 2016. Ultrathin flexible planar crystalline-silicon/polymer hybrid solar cell with 5.68% efficiency by effective passivation. Appl. Surf. Sci. 366, 494–498.

Liu, J., Ji, Y., Liu, Y., Xia, Z., Han, Y., Li, Y., Sun, B., 2017a. Doping-free asymmetrical silicon heterocontact achieved by integrating conjugated molecules for high efficient solar cell. Adv. Energy Mater. 7 (19), 1700311.

Liu, Y., Zhang, J., Wu, H., Cui, W., Wang, R., Ding, K., Lee, S.-T., Sun, B., 2017b. Low-temperature synthesis TiO_x passivation layer for organic-silicon heterojunction solar cell with a high open-circuit voltage. Nano Energy 34, 257–263.

Liu, Y., Zhang, Z.-G., Xia, Z., Zhang, J., Liu, Y., Liang, F., Li, Y., Song, T., Yu, X., Lee, S.-T., Sun, B., 2016. High performance nanostructured silicon-organic quasi p-n junction solar cells via low-temperature deposited hole and electron selective layer. ACS Nano 10 (1), 704–712.

Sahasrabudhe, G., Rupich, S.M., Jhaveri, J., Berg, A.H., Nagamatsu, K., Man, G., Chabal, Y.J., Kahn, A., Wagner, S., Sturm, J.C., Schwartz, J., 2015. Low-temperature synthesis of a TiO_2/Si heterojunction. J. Am. Chem. Soc. 137 (47), 14842–14845.

Tecedor, M.G., Karazhanov, S., Vasquez, G.C., Haug, H., Maestre, D., Cremades, A., González, M.T., Ramírez-Castellanos, J., González-Calbet, J.M., Piqueras, J., You, C.C., Marstein, E.S., 2018. Silicon surface passivation by PEDOT: PSS functionalized by SnO_2 and TiO_2 nanoparticles. Nanotechnology 29 (3), 035401.

Thomas, J.P., Leung, K.T., 2014. Defect-minimized PEDOT:PSS/planar-Si solar cell with very high efficiency. Adv. Funct. Mater. 24 (31), 4978–4985.

Tong, H., Yang, Z., Wang, X., Liu, Z., Chen, Z., Ke, X., Sui, M., Tang, J., Yu, T., Ge, Z., Zeng, Y., Gao, P., Ye, J., 2018. Dual functional electron-selective contacts based on silicon oxide/magnesium: tailoring heterointerface band structures while maintaining surface passivation. Adv. Energy Mater. 8 (16).

Wan, Y., Gao, M., Li, Y., Guo, H., Li, Y., Xu, F., Ma, Z., 2017. First principle study of ternary combined-state and electronic structure in amorphous silica. Acta Phys. Sin. 66 (18).

Xia, Z., Li, P., Liu, Y., Song, T., Bao, Q., Lee, S.-T., Sun, B., 2017. Black phosphorus induced photo-doping for high-performance organic-silicon heterojunction photovoltaics. Nano Res. 10 (11), 3848–3856.

Zhang, Y., Cui, W., Zhu, Y., Zu, F., Liao, L., Lee, S.-T., Sun, B., 2015. High efficiency hybrid PEDOT:PSS/nanostructured silicon Schottky junction solar cells by doping-free rear contact. Energy Environ. Sci. 8 (1), 297–302.